END

FILMED

MICROCOPY RESOLUTION TEST CHART
NATIONAL BUREAU OF STANDARDS-1963-A

Prepared for

SPACE DIVISION
AIR FORCE SYSTEMS COMMAND
Los Angeles Air Force Station
P.O. Box 92960, Worldway Postal Center
Los Angeles, Calif. 90009

82 11 26 012

A

This report was submitted by The Aerospace Corporation, El Segundo, Calif. 90245, under Contract No. F04701-81-C-0082 with the Space Division, Deputy for Technology, P.O. Box 92960, Worldway Postal Center, Los Angeles, Calif. 90009. It was reviewed and approved for The Aerospace Corporation by H. R. Rugge, Director, Space Sciences Laboratory. Captain Gary M. Rowe, SD/YLTM was the project officer for Mission-Oriented Investigation and Experimentation (MOIE) Programs.

This report has been reviewed by the Public Affairs Office (PAS) and is releasable to the National Technical Information Service (NTIS). At NTIS, it will be available to the general public, including foreign nations.

This technical report has been reviewed and is approved for publication. Publication of this report does not constitute Air Force approval of the report's findings or conclusions. It is published only for the exchange and stimulation of ideas.
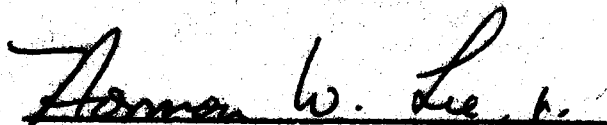

Gary M. Rowe, Captain, USAF
Project Officer

Jimmie H. Butler, Colonel, USAF
Director of Space Systems Technology

FOR THE COMMANDER

Norman W. Lee, Jr., Colonel, USAF
Deputy for Technology

REPORT DOCUMENTATION PAGE		READ INSTRUCTIONS BEFORE COMPLETING FORM
1. REPORT NUMBER SD-TR-82-67	2. GOVT ACCESSION NO. AD-A121 790	3. RECIPIENT'S CATALOG NUMBER
4. TITLE (and Subtitle) IN-FLIGHT CALIBRATION OF THE MONEX HIGH ENERGY SOLAR X-RAY MONITOR (HEM) ON THE P78-1 SATELLITE		5. TYPE OF REPORT & PERIOD COVERED
		6. PERFORMING ORG. REPORT NUMBER TR-0082(2940-01)-8
7. AUTHOR(s) Sharad R. Kane, Peter B. Landecker, and David L. McKenzie		8. CONTRACT OR GRANT NUMBER(s) F04701-81-C-0082
9. PERFORMING ORGANIZATION NAME AND ADDRESS The Aerospace Corporation El Segundo, Calif. 90245		10. PROGRAM ELEMENT, PROJECT, TASK AREA & WORK UNIT NUMBERS
11. CONTROLLING OFFICE NAME AND ADDRESS Space Division Air Force Systems Command Los Angeles, Calif.		12. REPORT DATE 1 September 1982
		13. NUMBER OF PAGES 40
14. MONITORING AGENCY NAME & ADDRESS(if different from Controlling Office)		15. SECURITY CLASS. (of this report) Unclassified
		15a. DECLASSIFICATION/DOWNGRADING SCHEDULE

16. DISTRIBUTION STATEMENT (of this Report)

Approved for public release; distribution unlimited.

17. DISTRIBUTION STATEMENT (of the abstract entered in Block 20, if different from Report)

18. SUPPLEMENTARY NOTES

19. KEY WORDS (Continue on reverse side if necessary and identify by block number)

Solar Flares
Solar X-Rays
X-Ray Detectors

20. ABSTRACT (Continue on reverse side if necessary and identify by block number)

Simultaneous observations of seven medium and large solar X-ray bursts made with the MONEX High Energy Monitor (HEM) on the P78-1 satellite and the X-Ray Spectrometer aboard the ISEE-3 (International Sun Earth Explorer-3) spacecraft have been used to examine the detector gain and response characteristics of the HEM instrument. It has been found that the HEM detector gain decreased by approx. 25% after the launch and subsequently decreased slowly with time. The gain was 72% and 66% of its pre-launch value about 5 weeks and 15 months after the launch, respectively. At total counting rates higher than 19000 (10^4) counts/sec

DD FORM 1473
(FACSIMILE)

Cont'd

18. KEY WORDS (Continued)

20. ABSTRACT (Continued)

there is a large decrease in the detector gain resulting in an apparent counting rate saturation. The overall instrument performance appears to be satisfactory and it is expected that the HEM observations will be useful in the study of many small and medium intensity solar X-ray bursts.

CONTENTS

FIGURES

TABLES

I. INTRODUCTION

During the past decade it has become apparent that energetic electrons (> 10 keV) play a major role in the solar flare process. Especially during the impulsive phase, they seem to carry a substantial part of the released flare energy and transport it to the sources of X-ray, EUV, optical and radio emissions (Kane et al., 1980). The properties of these energetic electrons can be deduced through observations of the hard X-ray bremsstrahlung they produce as they interact with the ambient solar atmosphere. Therefore a High Energy X-Ray Monitor (HEM) was included in the Aerospace Corporation solar instrument package aboard the U. S. Air Force P78-1 satellite.

Since the launch of P78-1 on 24 February 1979, the HEM has recorded many large and small hard X-ray bursts associated with solar flares. As in the case of most instruments, proper interpretation of these observations depends critically on our understanding of the response characteristics of the HEM to the variety of X-ray spectra produced in solar flares. This, in turn, requires an analysis of the computed and observed response in the laboratory prior to the launch as well as possible changes in the detector gain during and after the launch. Since no on-board calibration source is available for in-flight calibration of the HEM, it is necessary to compare the HEM observations of solar flares with simultaneous observations made with another comparable instrument for which in-flight calibration is available. One such instrument, the X-Ray Spectrometer aboard the ISEE-3 (International Sun Earth Explorer-3) spacecraft (Kane et al., 1982), was in operation at the time of the launch of P78-1 and has several simultaneous flare observations with the HEM. Seven of these flare observations have now been analyzed. The purpose of this report is to present the results of that analysis relevant to the response characteristics of the HEM for solar flare observations.

II. INSTRUMENTATION

The MONEX High Energy X-Ray Monitor (HEM) is a part of The Aerospace
Corporation's X-ray experiment package on the U. S. Air Force Space Test
Program satellite P78-1. It has been described earlier by Landecker, McKenzie
and Rugge (1979) and Landecker et al. (1979). The HEM consists of a
proportional counter, 28.7 cm^2 in effective area and filled with a mixture of
97% Xenon and 3% CO_2 to a pressure of 3.0 atm. The entrance window is made of
0.11 cm thick aluminum and is designed to absorb the incident flux of X-rays
of energy less than 10 keV. The spectral resolution is ~ 10% FWHM for ~ 22
keV X-rays. The nominal X-ray energy range of 11-140 keV is covered with six
energy channels (Table 1). The exact value of the X-ray energy range depends
on the detector gain. The high voltage across the counter and hence its gain
can be set to one of two possible values, "normal" or "high," through ground
commands. The ratio of gains (measured prior to launch) at "high" vs.
"normal" high voltage equals 1.63. Except for the short period from 26
February (0800 UT) to 10 March (0506 UT) 1981, the high voltage was set to the
"normal" value.

HEM measures the X-ray flux from the whole solar disc. The time
resolution for the integral flux of 11-140 keV X-rays is 0.032 sec; a six-
channel differential X-ray spectrum is also measured in this energy range with
1.024 sec time resolution.

In order to deduce the incident X-ray spectrum from the observed counting
rates of the six energy channels, it is necessary to know the corresponding
geometry factors (cm^2 keV). In general, the geometry factors depend on the
detector geometry, gas filling, and entrance window as well as the detector

9

Table 1

X-RAY ENERGY CHANNELS FOR GAIN = 1.00

Channel No.	Energy Range (keV)	Mid-Point Energy (keV)
	11.3 - 14.6	13.0
	14.6 - 20.1	17.5
	20.3 - 27.7	24.0
	27.7 - 36.7	32.2
	36.3 - 52.3	44.5
	52.3 - 140.0	96.2

gain, spectral resolution and the hardness of the X-ray spectrum. The geometry factors for the six energy channels have been computed for thermal spectra with different temperatures and non-thermal (power law, $\sim E^{-\gamma}$) spectra with different spectral exponents. These calculations have been performed for a variety of detector gains between 0.3 and 1.0, the gain of 1.0 corresponding to the nominal values of the X-ray energy channels given in Table 1. As an example, Fig. 1 shows the geometry factors for the values of the power law spectral index γ between 1 and 6, for the case of the detector gain being 0.56. It can be seen that, in general, the geometry factor varies with γ. However, for the first five energy channels this dependence on γ is relatively small ($< 30\%$) provided $1 \lesssim \gamma \lesssim 5$. On the other hand, the geometry factor for the sixth (highest energy) channel increases by as much as a factor of ~ 5.6 for an increase in γ from 1 to 5. This is due to a spillover from the lower energy channels when the input X-ray spectrum is steep.

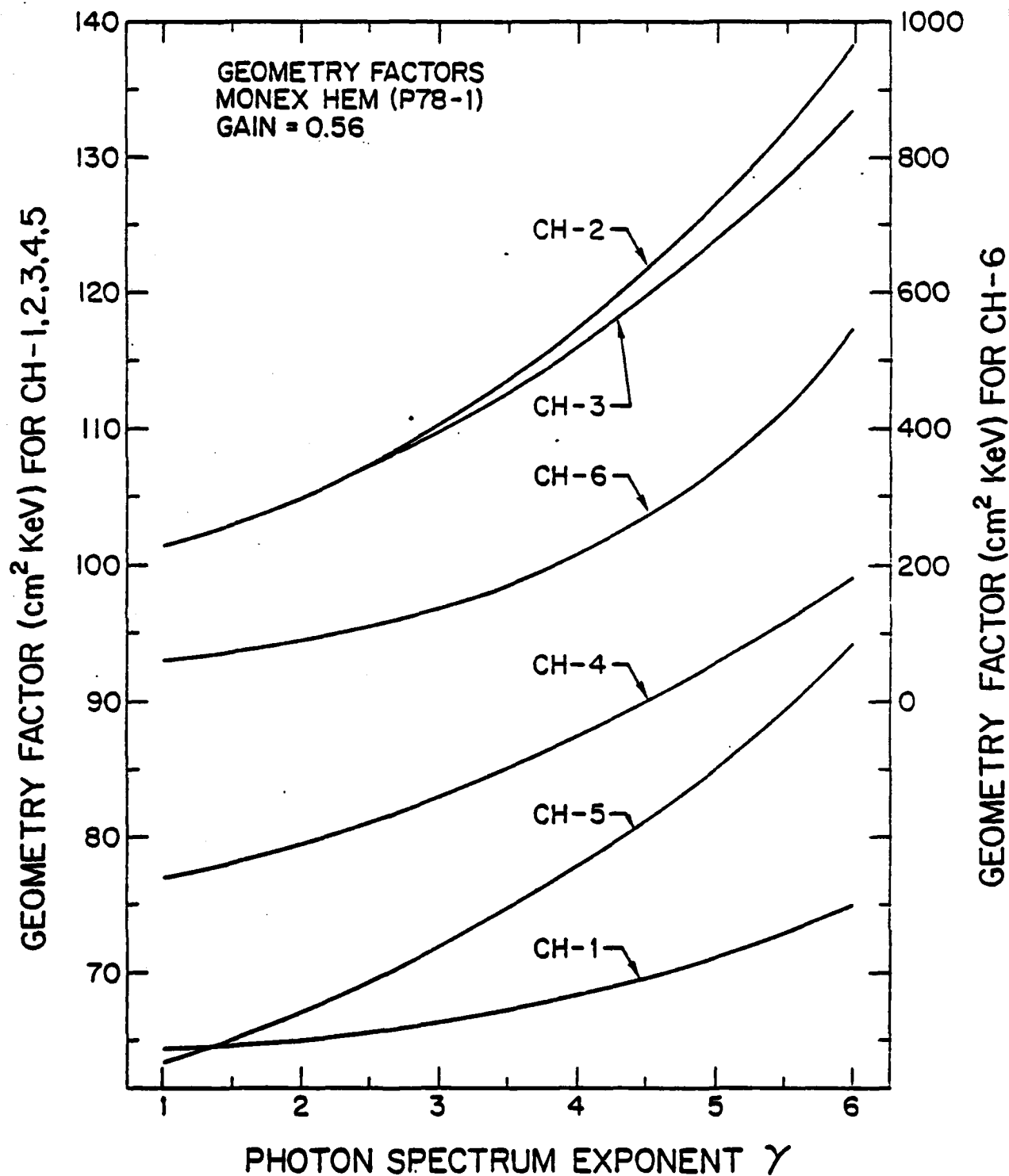**Figure 1:** Geometry factors in cm^2-keV for the six MONEX HEM energy channels plotted as a function of the exponent of an assumed photon flux spectrum of the form $F(E) = AE^{-\gamma}$.

12

III. OBSERVATIONS

The P78-1 satellite was launched on 24 February 1979. Since then the HEM has observed many solar X-ray bursts. Examples have been published earlier (cf. Landecker and McKenzie, 1981, and references therein). For the present study it was necessary to select events which were most suitable for obtaining the in-flight calibration and response characteristics. Specifically the selection was based on the following criteria:

1. Neglible contamination of the HEM data from the earth's radiation belts.

2. Simultaneous observations by ISEE-3 available.

3. Peak X-ray flux large enough so that X-ray spectra could be deduced from both HEM and ISEE-3 instruments.

4. Events to cover a wide range of peak X-ray fluxes.

5. Events to be well distributed in time of occurrence.

The last two criteria were designed so that a possible dependence of the HEM response on the magnitude and spectrum of incident X-ray flux and on the time elapsed since launch could be examined.

During the period March 1979 - June 1980 six events were found to satisfy these criteria. At the time of these events the high voltage was set to the "normal" value. We selected an additional event, on 26 February 1981, for which the high voltage was set to the "high" value. In this way it was hoped that the effect of high voltage setting on the detector gain could also be examined.

The seven solar flare events selected for the present study are presented in Table 2 and Figures 2 through 8. The total detector counting rate at the peak of these events varies from 4.0×10^3 counts/sec to 1.2×10^4 counts/sec. The rate vs. time profile also varies a great deal from one event to another. For example, the 5 November 1979 event is a relatively simple and small X-ray burst with only one prominent maximum. On the other hand, the X-ray burst on 7 June 1980 shows large intensity variations with seven peaks and valleys.

Table 2

EVENTS USED FOR IN-FLIGHT CALIBRATION OF THE HEM

Date	Time of Max (UT)	Flare X-Ray Class	Peak Ch-1	Rate Ch-2	(Counts/Sec) CH-3	Total	High Voltage Setting	Deduced Gain (fraction of nominal)
3 Apr 1979	0417:17	M4	833	1601	1051	4005	Normal	0.72
27 Apr 1979	0646:07	X1	4486	3272	1364	9910	Normal	0.62
5 Nov 1979	2149:01	M4	2678	1828	692	5591	Normal	0.62
9 Nov 1979	0304:43*	M9	3986	4035	1994	11953	Normal	0.62
29 Mar 1980	0918:13	C9	2223	2567	1063	6479	Normal	0.56
7 Jun 1980	0312:15	M7	3136	3359	1399	8948	Normal	0.56
26 Feb 1981	1425:18*	X1.8	4792	4602	1759	12136	High	0.47

*May not be true maximum.
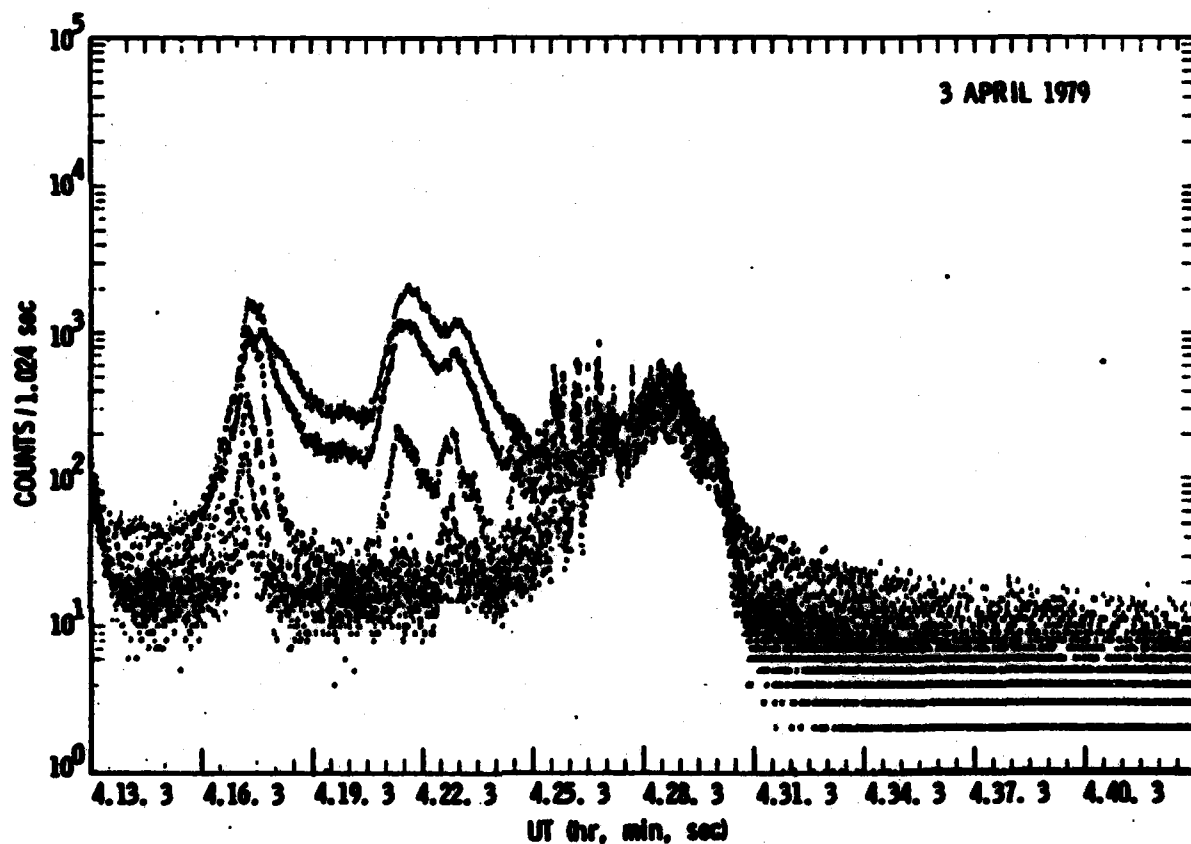
Figure 2: HXM channel counting rates (counts/1.024 s) plotted as a function of time for the X-ray flare of 3 April 1979. Each data point for channel n is plotted as a small numeral n. Starting at about UT 04:25 charged particle background dominates the counting rate.

Figure 3:   HXM channel counting rates near the peak of the 27 April 1979 flare.

Figure 4:   HXM channel counting rates for the 5 November 1979 flare.

Figure 5:   HEM channel counting rates for the 9 November 1979 flare.

Figure 6: HXM channel counting rates for the 29 March 1980 flare.

Figure 7: HXM channel counting rates for the 7 June 1980 flare.

Figure 8:   HEM channel counting rates for the 26 February 1981 flare.

IV. DETECTOR GAIN

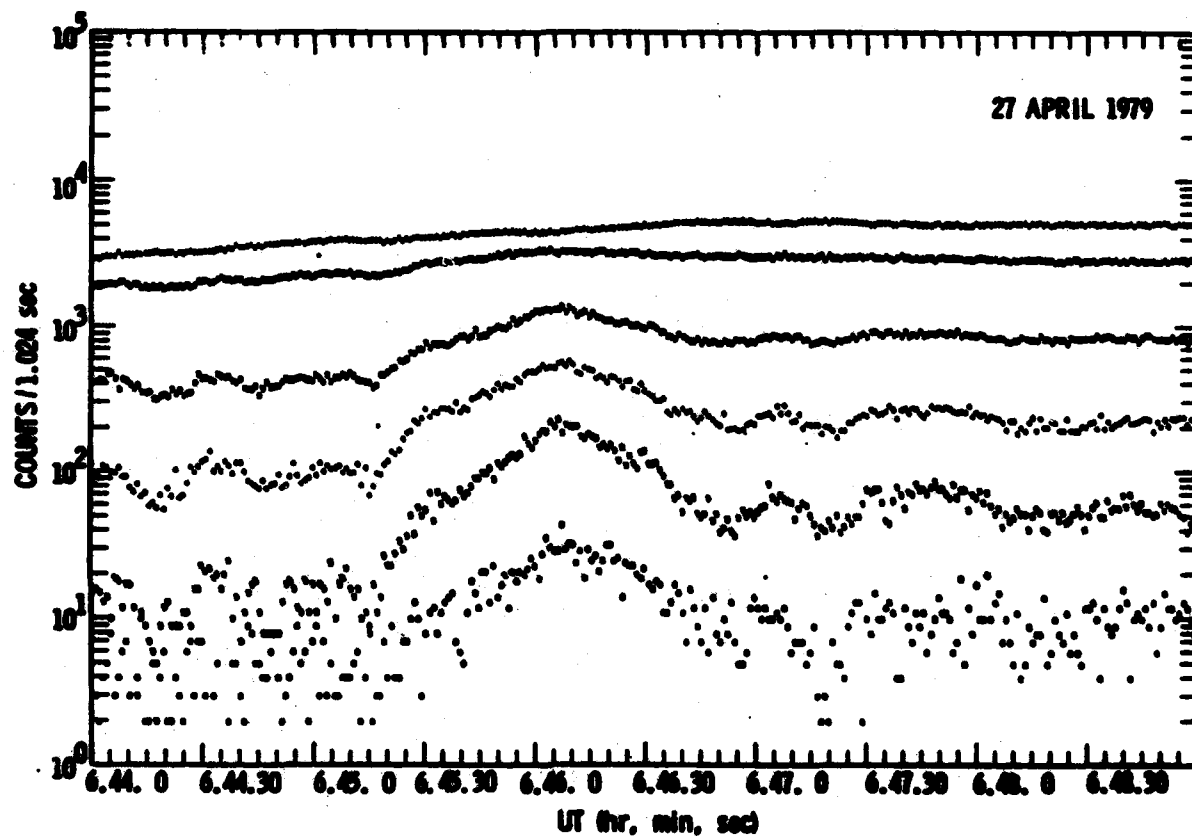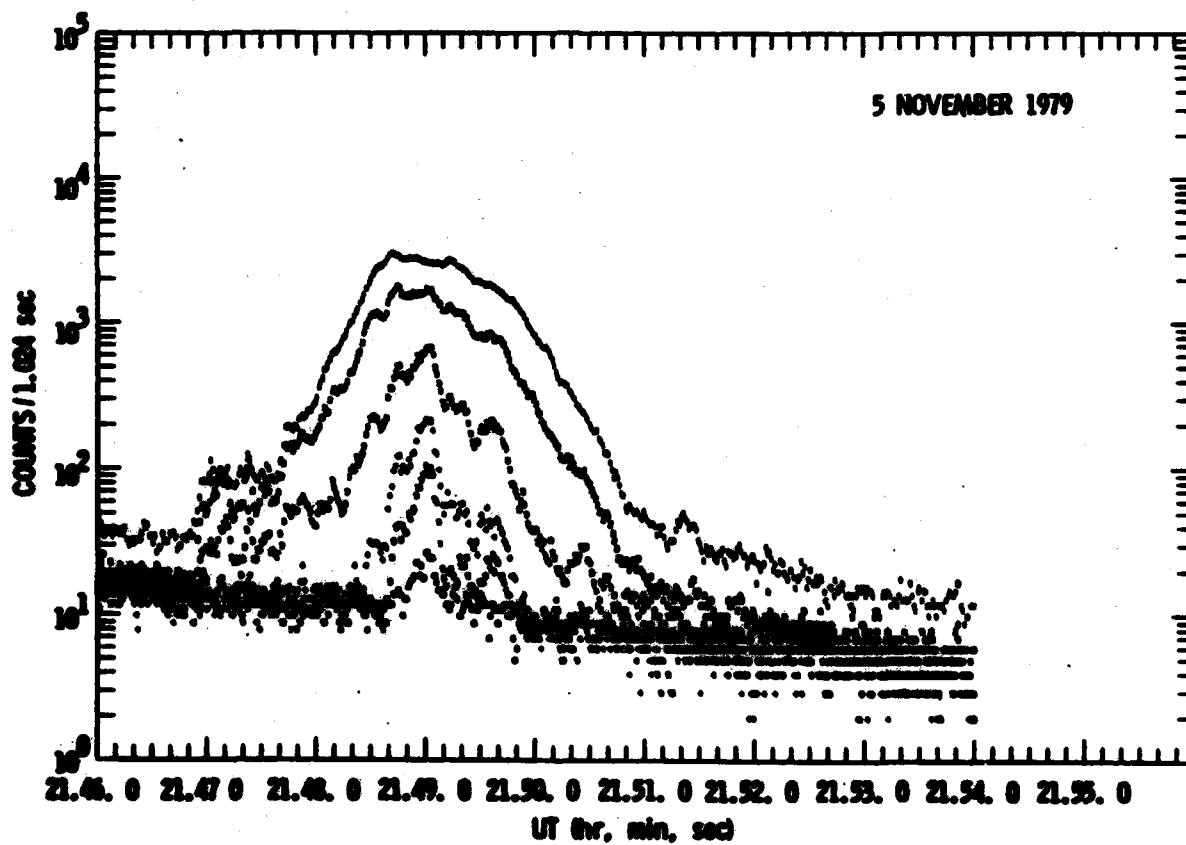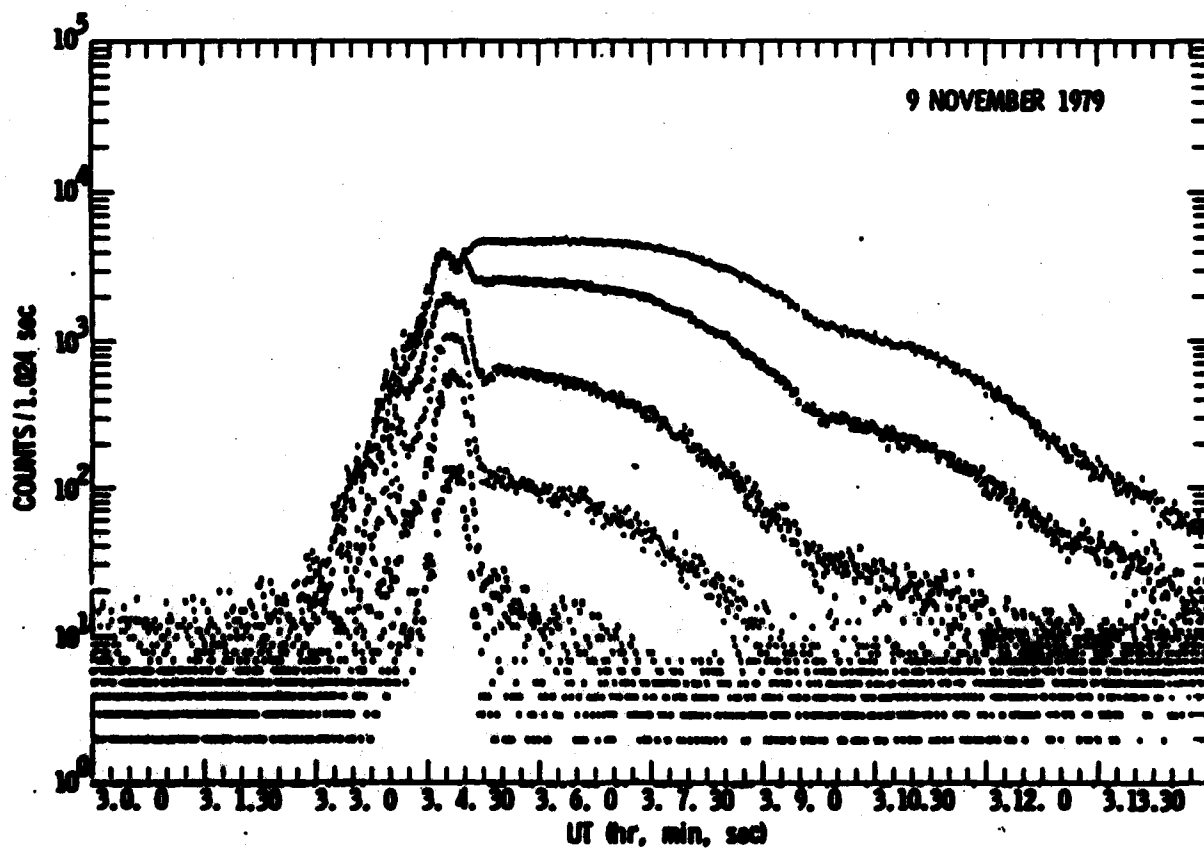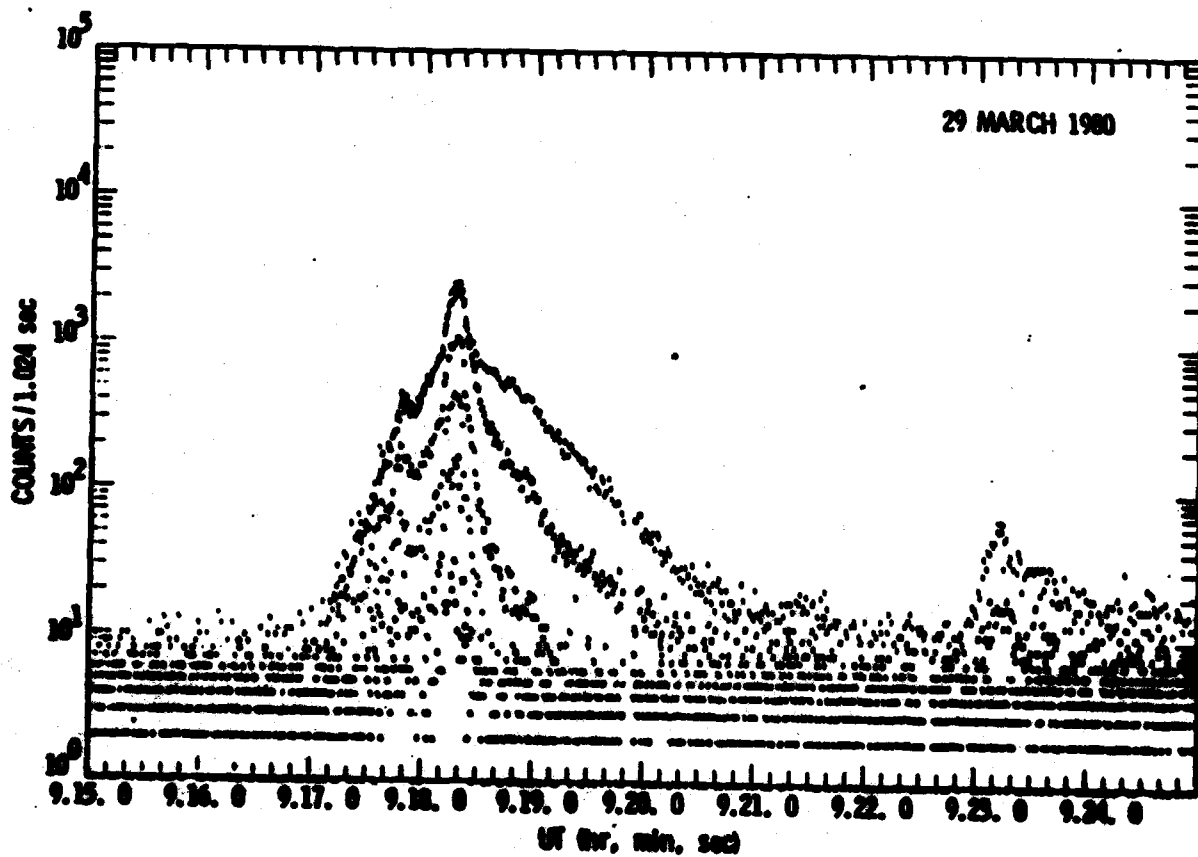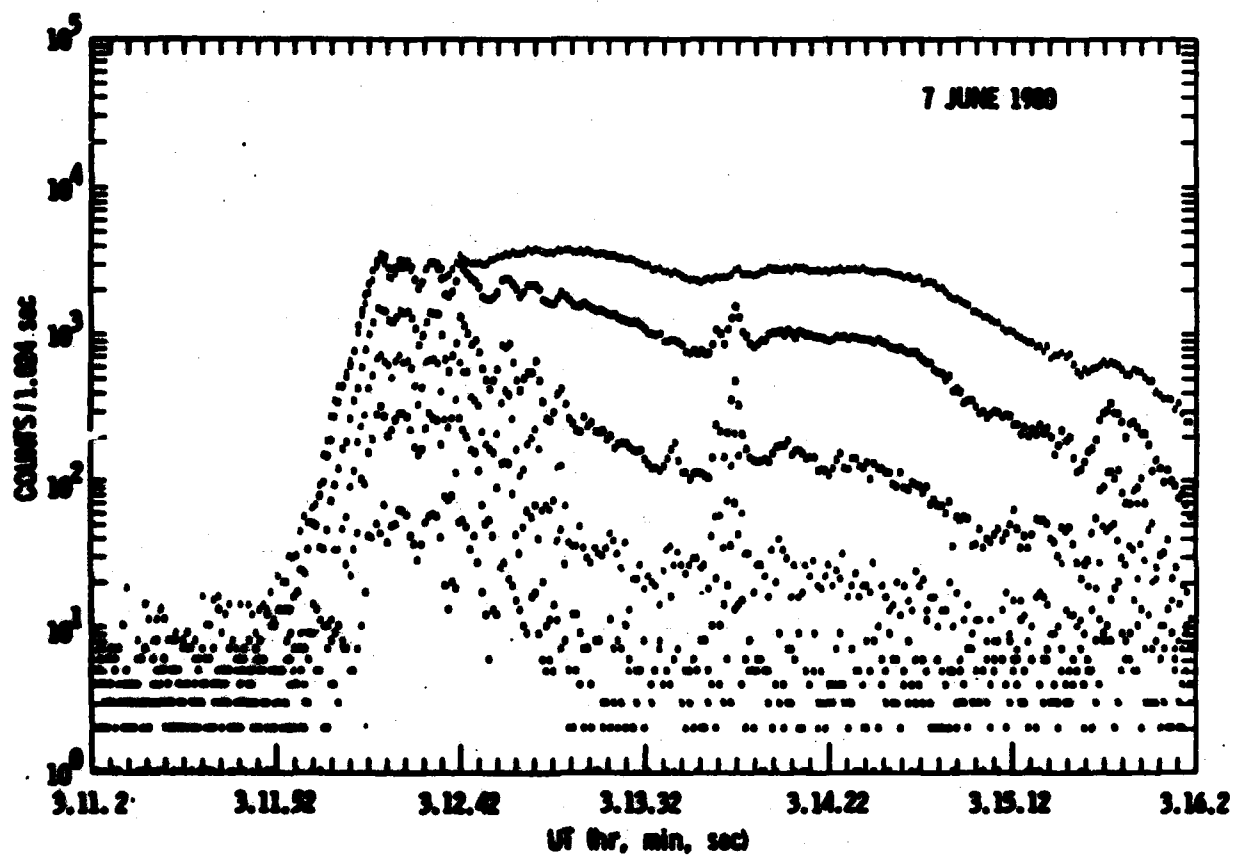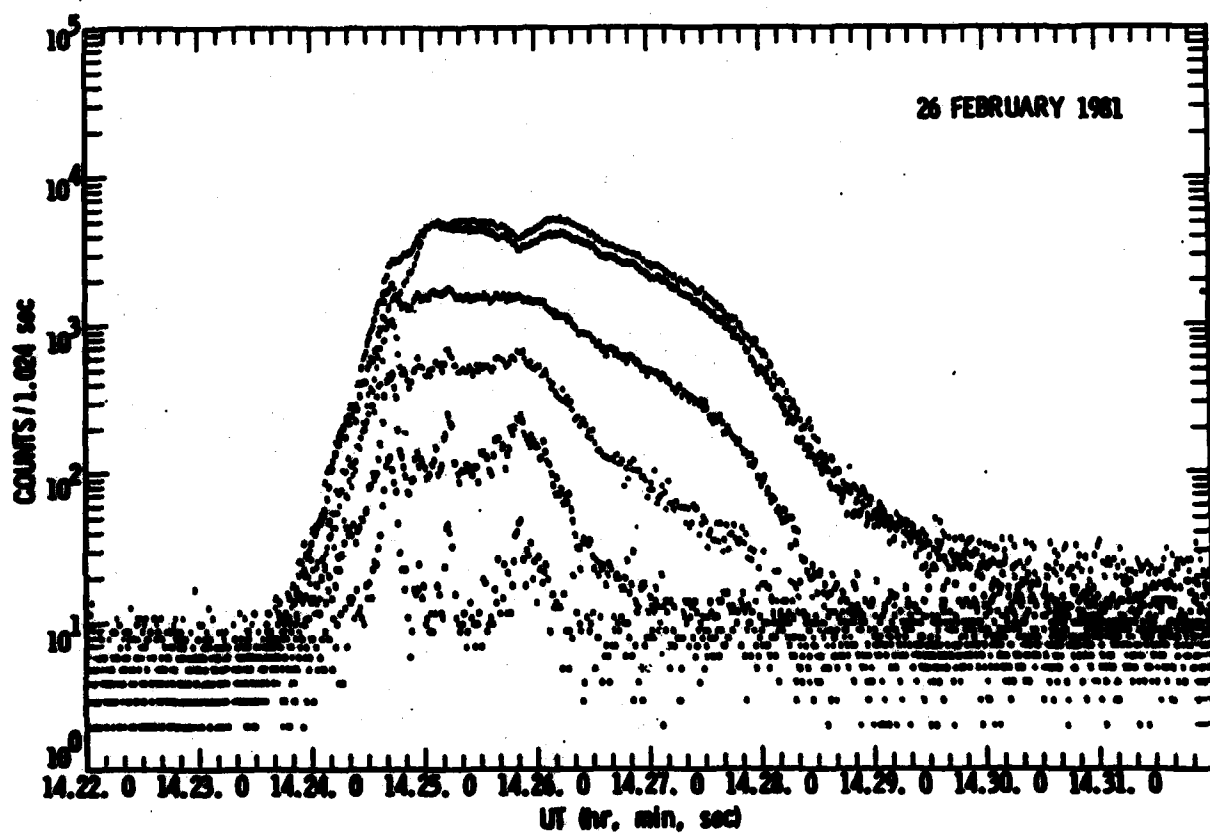A preliminary comparison of the HEM and ISEE-3 observations showed that the HEM was responding to much higher energy X-rays than those expected from Table 1. This indicated that the HEM detector gain decreased substantially after the launch. Moreover, in large flares, the gain appeared to change with time during a single event if the X-ray flux was above a certain value. Since there is no indicator of the detector gain in the HEM data, the following procedure was adopted for deducing the true gain and hence the X-ray energy response.

1. In each of the seven events in Table 2, two times were selected at which the X-ray fluxes were large enough so that the X-ray spectrum could be obtained from the ISEE-3 observations. These times were usually close to the X-ray maximum. In order to obtain good statistical accuracy, 4-sec averages of the X-ray data were used in most cases. As suggested by the earlier observations made with other spacecraft (cf. Kane and Anderson, 1970; Frost and Dennis, 1971), the X-ray spectrum incident on the detector was assumed to be a double power law of the form

$$\frac{dJ}{dE} = \begin{cases} K_1 \; E^{-\gamma_1} \text{ for } E < E_0 \text{ keV} \\ K_2 \; E^{-\gamma_2} \text{ for } E > E_0 \text{ keV} \end{cases}$$
$$\text{photons cm}^{-2} \text{ sec}^{-1} \text{ keV}^{-1} \; ,$$

where $K_2 = K_1 \; E_0^{(\gamma_2 - \gamma_1)}$. The counting rates of the twelve X-ray energy channels of the ISEE-3 instrument due to the above incident X-ray spectrum were computed on the basis of the known response characteristics. The four parameters K_1, γ_1, γ_2 and E_0 of the incident spectrum were varied until the best possible agreement (as indicated by χ^2) could be obtained between the

23

computed and observed counting rates. For a graphical presentation of the observed spectrum, the ISEE-3 counting rates were divided by the corresponding geometry factors to give the X-ray flux in photons cm^{-2} sec^{-1} keV^{-1} ("ISEE-3 X-ray spectrum").

2. The incident X-ray spectrum thus deduced from the ISEE-3 measurements was used to obtain the relevant spectral index and the corresponding geometry factor for each of the six X-ray energy channels of the HEM instrument for an assumed value of the HEM detector gain. The "HEM X-ray spectrum" was then obtained by dividing the observed counting rates by the corresponding geometry factors.

3. The "HEM X-ray spectrum" was compared with the "ISEE-3 X-ray spectrum" by plotting the two together on a log-log plot of photon flux vs. photon energy. In case of a disagreement between the two spectra, a different value was assumed for the gain of the HEM detector and the geometry factors were recomputed. This procedure was repeated until a satisfactory agreement was obtained between the ISEE-3 and HEM X-ray spectra. Whether the agreement is satisfactory or not was based on a visual inspection of the HEM data points relative to the ISEE-3 X-ray spectrum. This was considered adequate for the present purpose because of the uncertainties in the deduced X-ray spectrum due to the lower spectral resolution of the ISEE-3 instrument and the uncertainties in the HEM instrument, such as possible changes in the spectral resolution after the launch.

Figures 9 through 15 show the results for the seven solar flare events mentioned in Table 2. In each case the assumed value of the HEM detector gain is also indicated. This was the gain for which a satisfactory agreement could be found between the ISEE-3 and HEM X-ray spectra. The solid line represents

24
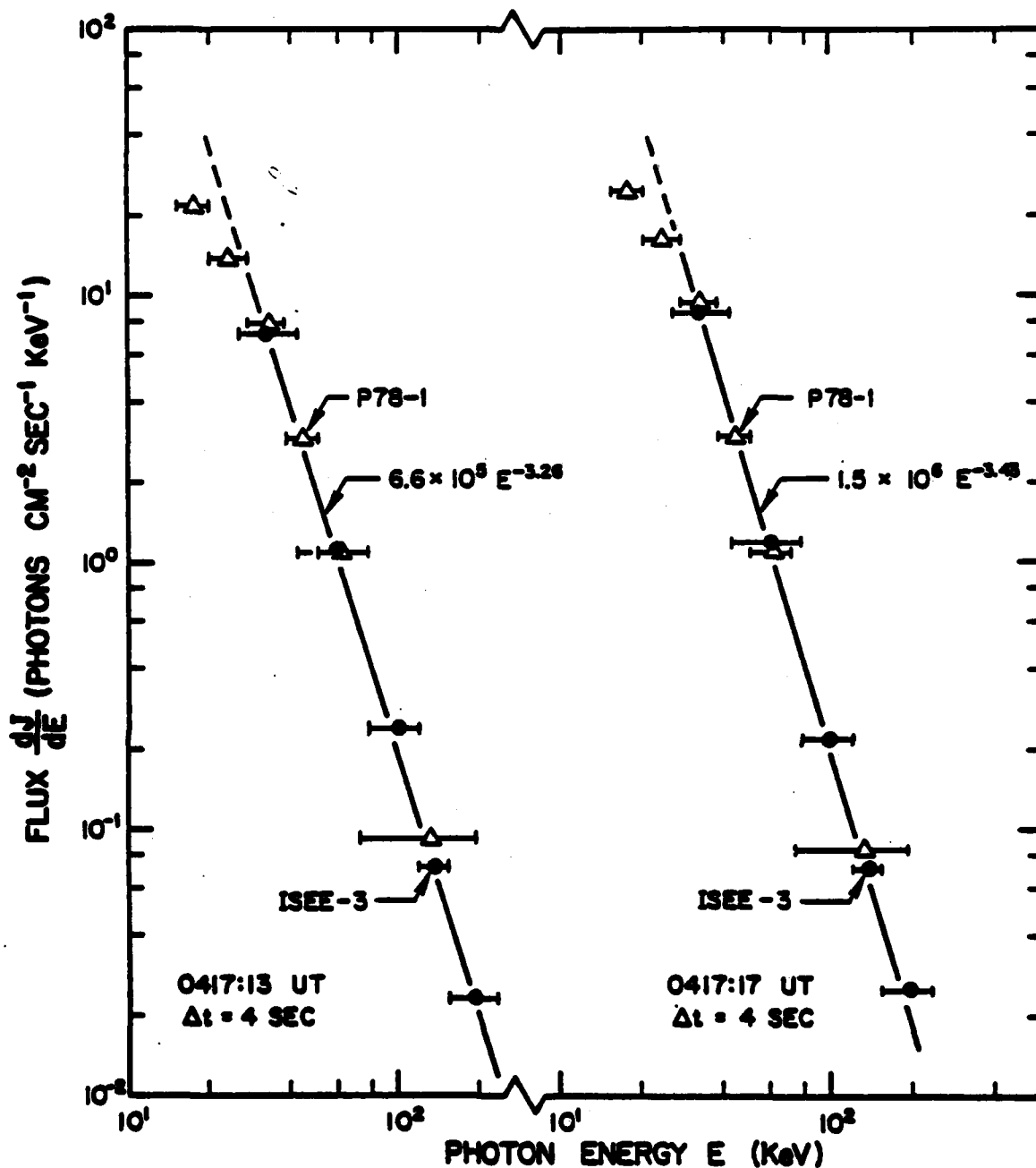
Figure 9: X-ray spectra from a solar flare on 3 April 1979 as measured by the MONEX HEM (P78-1) and the ISEE-3 detectors. The HEM spectra were obtained by varying the assumed gain until agreement with the ISEE-3 fits (solid lines) was obtained. The inferred HEM gain was 0.72 times the prelaunch value.

SOLAR X-RAYS - 27 APRIL 1979
(P78-1 GAIN = 0.62)

FLUX $\frac{dJ}{dE}$ (PHOTONS CM^{-2} SEC^{-1} KeV^{-1})

10^2

10^1

10^0

10^{-1}

10^{-2}

3.5×10^5 E$^{-2.73}$

P78-1

P78-1

1.7×10^6 E$^{-3.20}$

ISEE-3

ISEE-3

9.9×10^7 E$^{-4.05}$

0646:02 UT
$\Delta t = 4$ SEC

0646:14 UT
$\Delta t = 4$ SEC

10^1 10^2 10^1 10^2

PHOTON ENERGY E (KeV)

Figure 10:   X-ray spectra from a flare on 27 April 1979, as measured by the
HEM and the ISEE-3 detectors.   The HEM gain was 0.62 times the
prelaunch value.

26
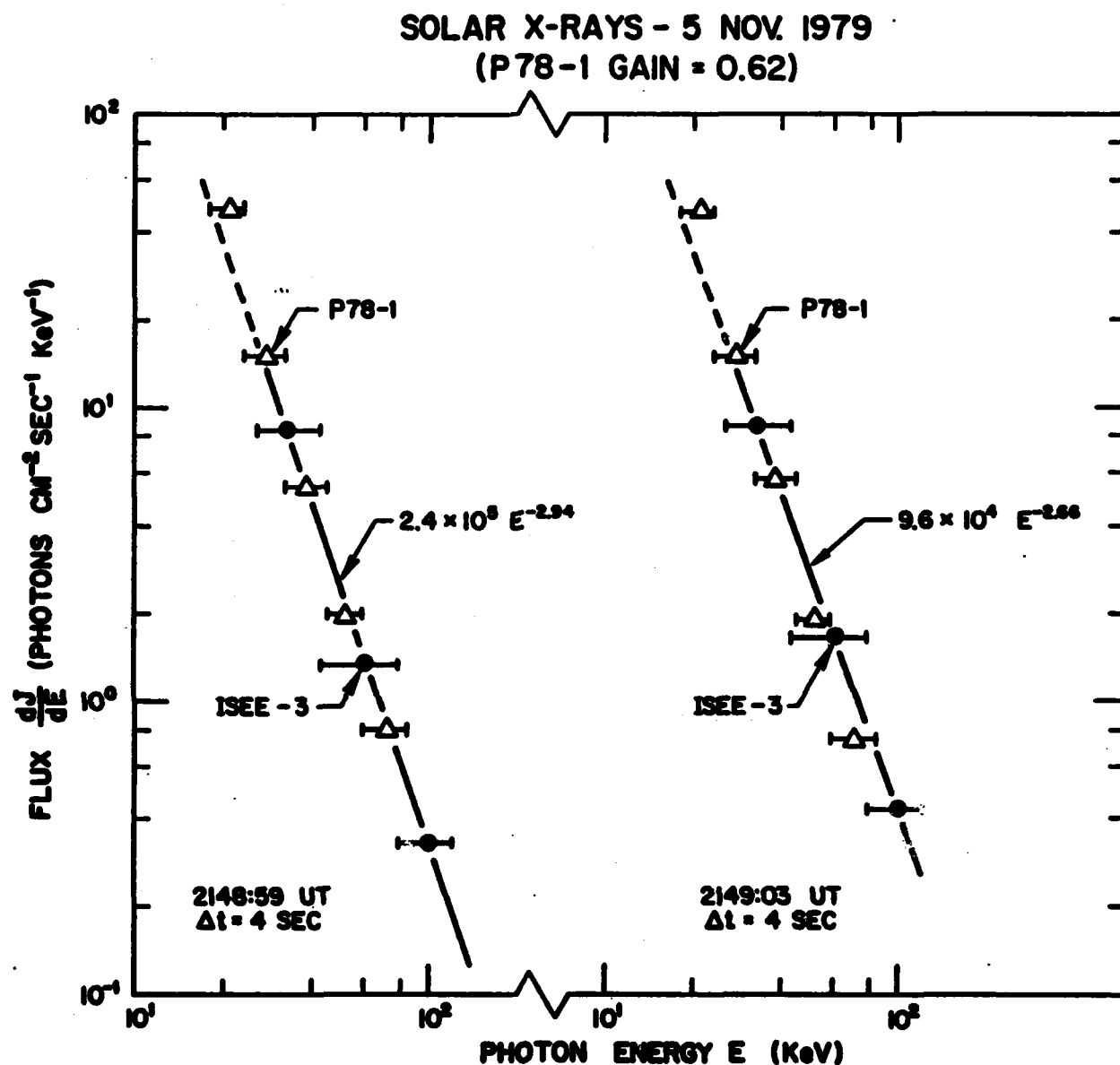
Figure 11: X-ray spectra from a flare on 5 November 1979, as measured by the HEM and the ISEE-3 detectors. The HEM gain was 0.62 times the prelaunch value.

SOLAR X-RAYS - 9 NOV. 1979
(P78-1 GAIN=0.62)
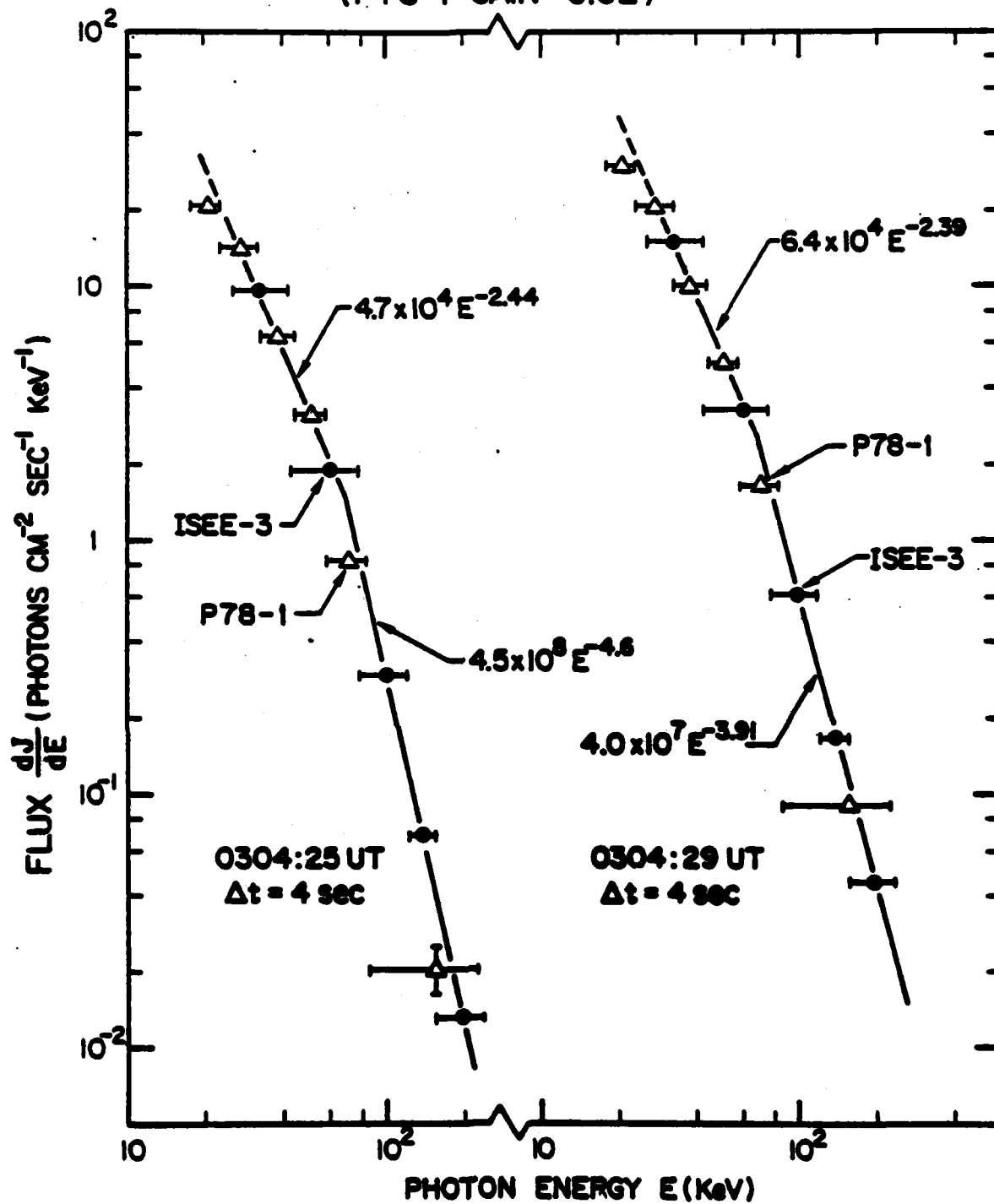
Figure 12: X-ray spectra from a flare on 9 November 1979, as measured by the HXM and the ISEE-3 detectors. The HXM gain was 0.62 times the prelaunch value.
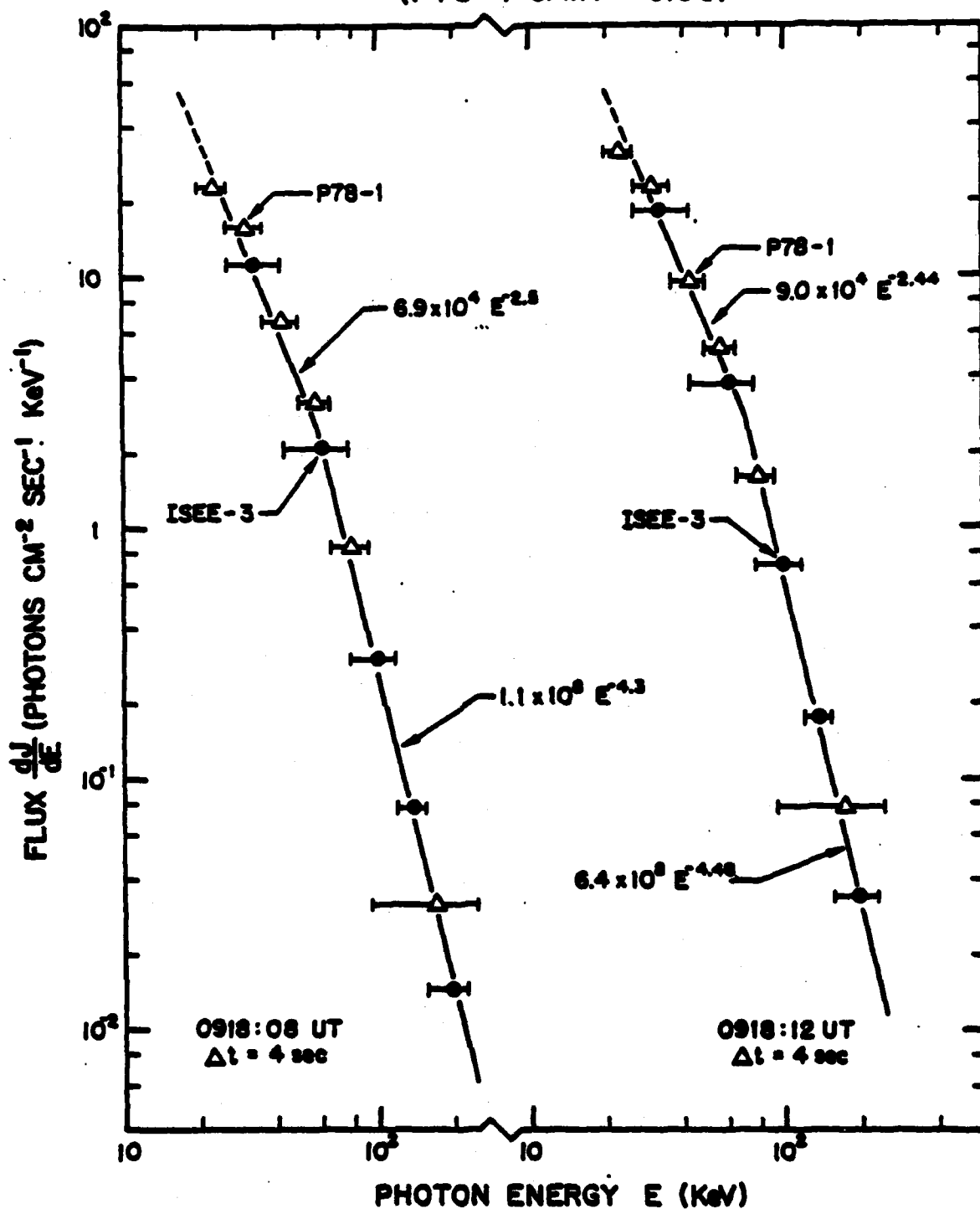
Figure 13: X-ray spectra from a flare on 29 March 1980, as measured by the HXM and the ISEE-3 detectors. The HXM gain was 0.56 times the prelaunch value.
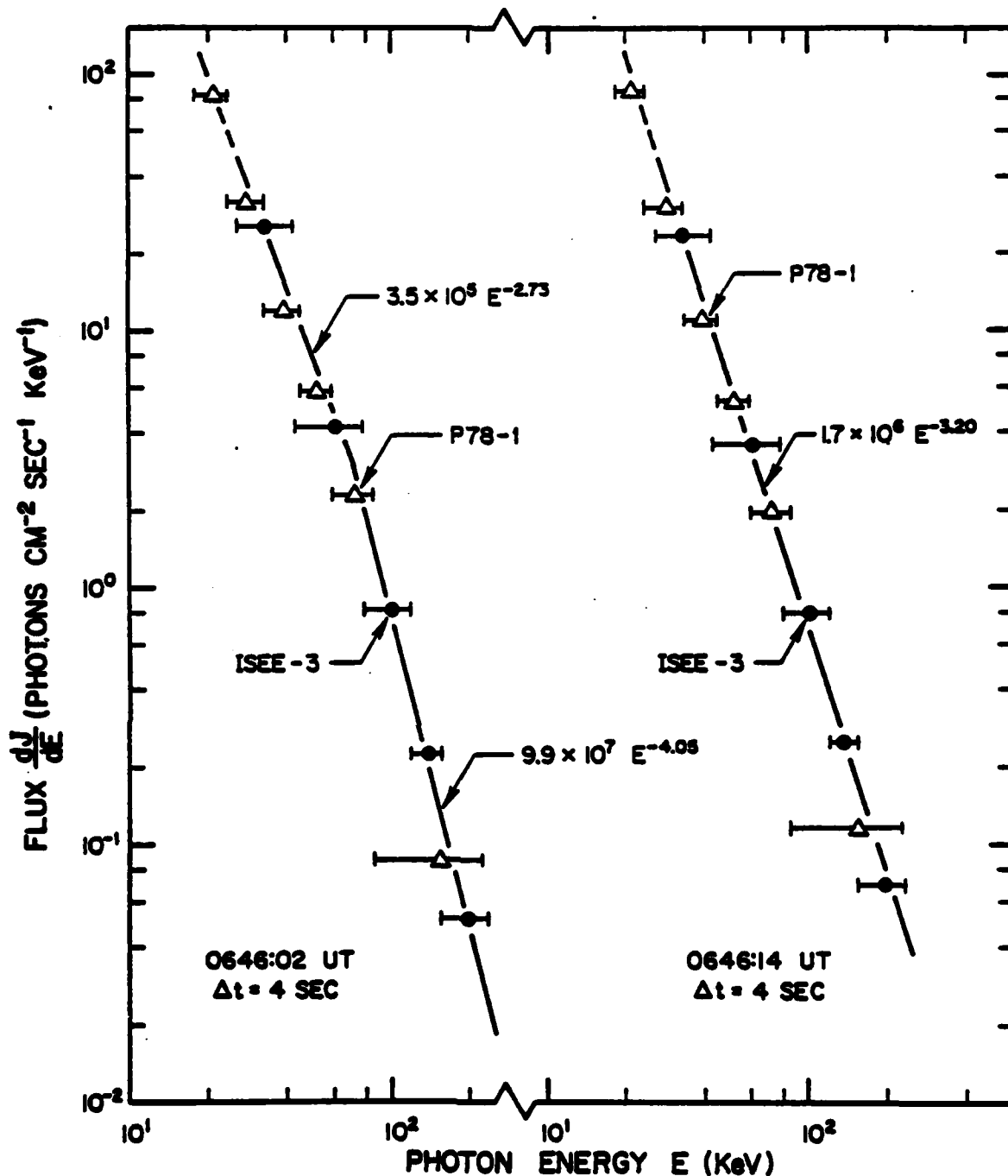
SOLAR X-RAYS – 7 JUNE 1980
(P78-1 GAIN = 0.56)
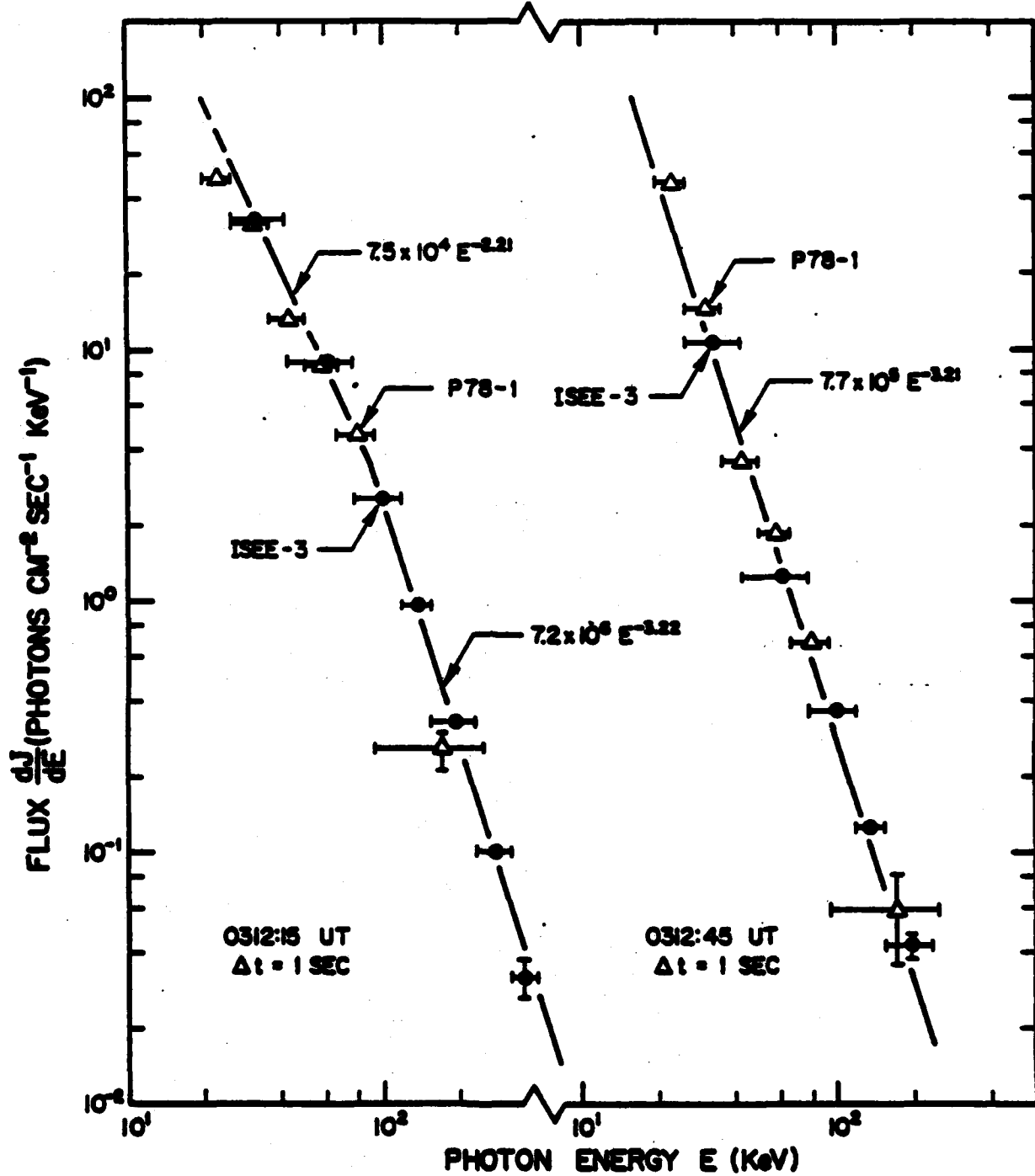
Figure 14: X-ray spectra from a flare on 7 June 1980, as measured by the HXM and the ISEE-3 detectors. The HXM gain was 0.56 times the pre-launch value.

SOLAR X-RAYS — 26 FEB. 1981
(P78-1 GAIN = 0.76)

$5.7 \times 10^4 E^{-2.37}$

P78-1

P78-1

$4.7 \times 10^6 E^{-3.48}$

$9.6 \times 10^5 E^{-3.13}$

ISEE-3

ISEE-3

1424:44 UT
$\Delta t = 4$ sec

1424:48 UT
$\Delta t = 4$ sec

FLUX $\frac{dJ}{dE}$ (PHOTONS CM^{-2} SEC^{-1} KeV^{-1})

PHOTON ENERGY E (KeV)
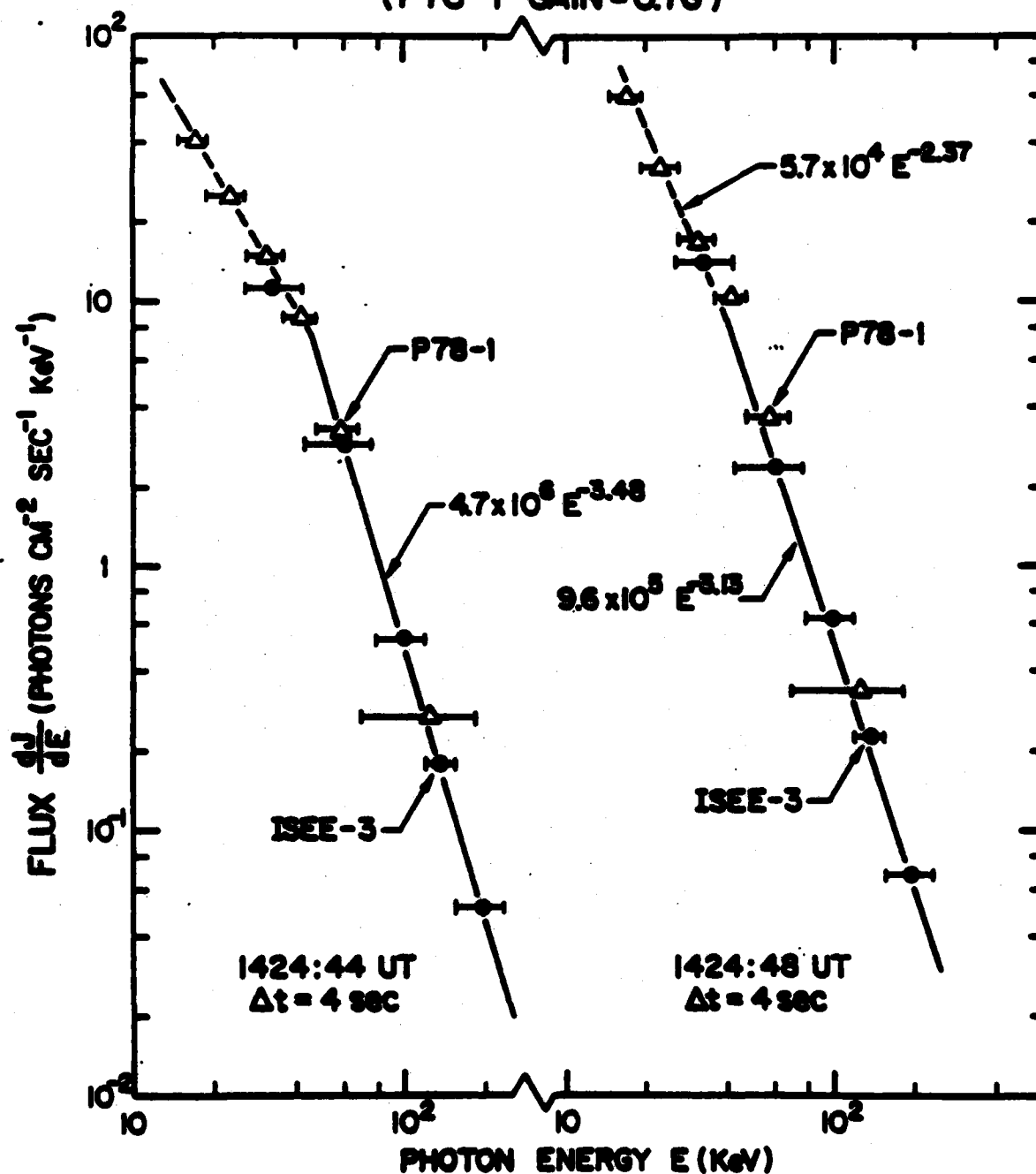
Figure 15: X-ray spectra from a flare on 26 February 1981, as measured by the HXM and ISEE-3 detectors. The HXM was in the high gain mode at this time. The gain of 0.76 times the prelaunch value corresponds to a normal mode gain of 0.47.

the X-ray spectrum deduced from the ISEE-3 measurements. The dashed line is an extrapolation of that spectrum to X-ray energies below 25 keV. In general there is a good agreement between the ISEE-3 and HEM spectra. In cases where the lower one or two energy channels of HEM fall on one side of the extrapolated ISEE-3 spectrum, as for example in Fig. 9, it is possible that the true X-ray spectrum itself is different from the extrapolated spectrum.

From the above comparison it is clear that the HEM detector gain decreased substantially after the launch of P78-1. On 3 April 1979, about five weeks after the launch, the gain was ~ 72% of its pre-launch value. Subsequently the gain decreased systematically with time, being ~ 56% of its pre-launch value on 7 June 1980. On 26 February 1981 the gain was ~ 76% of its pre-launch value. But this high value was due to the increased high voltage across the detector at that time. If the nominal pre-launch gain ratio of 1.63 is used, then the implied gain on 26 February 1981 was 47%. The gain as a function of time is shown in Table 2.

V. SATURATION EFFECTS

Two flare events in Table 2, viz. 9 November 1979 and 26 February 1981, produced total peak counting rates in the HEM detector which were in excess of 10^4 counts/sec. The X-ray spectra shown earlier in Figs. 12 and 15 were obtained at times when the total counting rates were much lower.

Fig. 16 shows a comparison of the HEM and ISEE-3 X-ray spectra at times of high counting rates in the 26 February 1981 event. Although the value of the gain used in Fig. 16 is the same as that in Fig. 15, all the HEM data points fall substantially below the ISEE-3 X-ray spectra. This indicates a decrease in the HEM detector gain at high counting rates. A similar effect was found in the 9 November 1979 event.

In order to determine the critical counting rate above which the HEM detector gain may decrease substantially, the HEM counting rates in the 9 November 1979 event were plotted against the counting rate of 26-43 keV X-rays recorded simultaneously by ISEE-3. The result is shown in Fig. 17. Four HEM channels covering 18-59 keV X-rays are shown separately. The two channels, 23.6 - 32.7 keV and 32.7 - 44.7 keV, are closest in energy to the ISEE-3 X-ray channel. The time interval covered is 0304:05 - 0304:53 UT, which corresponds to the rise of the X-ray flux to its maximum value.

From Fig. 17 it can be seen that the relationship between the HEM and ISEE-3 counting rates is linear for the 23.6 - 32.7 keV channel counting rates $< 2 \times 10^3$ counts/sec. The corresponding total counting rate of the HEM was $< 5.5 \times 10^3$ counts/sec. At higher rates the HEM - ISEE-3 relationship begins to be non-linear. This could be partly due to changes in the incident X-ray spectrum. At total HEM rates $> 10^4$ counts/sec the HEM response is saturated

SOLAR X-RAYS - 26 FEB. 1981
(P78-1 GAIN = 0.76)

10^3

10^2

2.5×10^{10} $E^{-3.91}$

ISEE-3

P78-1

5.4×10^6 $E^{-3.30}$

10

FLUX $\frac{dJ}{dE}$ (PHOTONS cm^{-2} SEC^{-1} KeV^{-1})

ISEE-3

P78-1

5.5×10^6 $E^{-3.63}$

1

10^{-1}

1425:52 UT
$\Delta t = 4$ sec

1425:56 UT
$\Delta t = 4$ sec

10^{-2}

10 10^2 10 10^2

PHOTON ENERGY E (KeV)
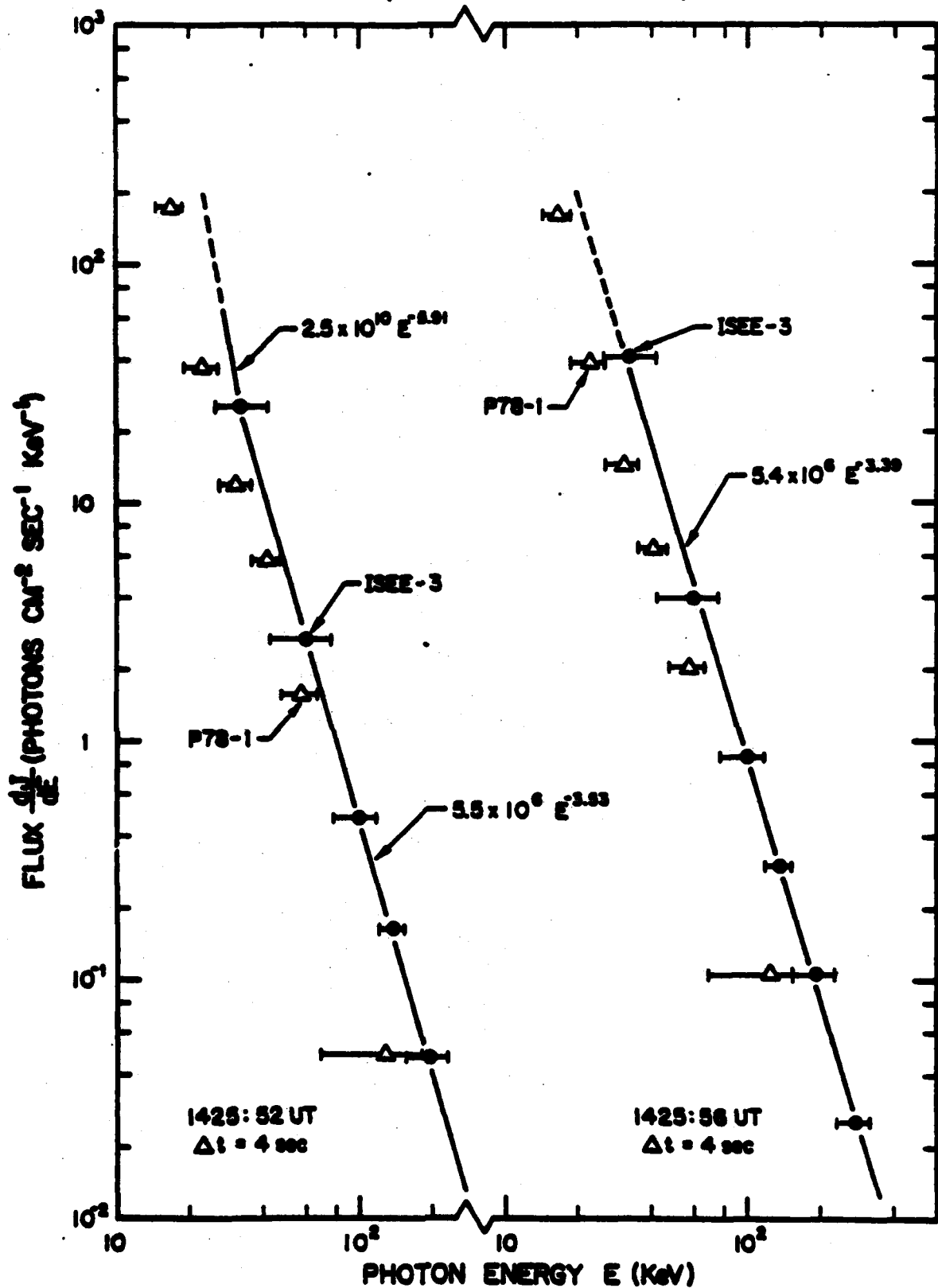
Figure 16: X-ray spectra from a flare on 26 February 1981 at times of high HXM counting rates.
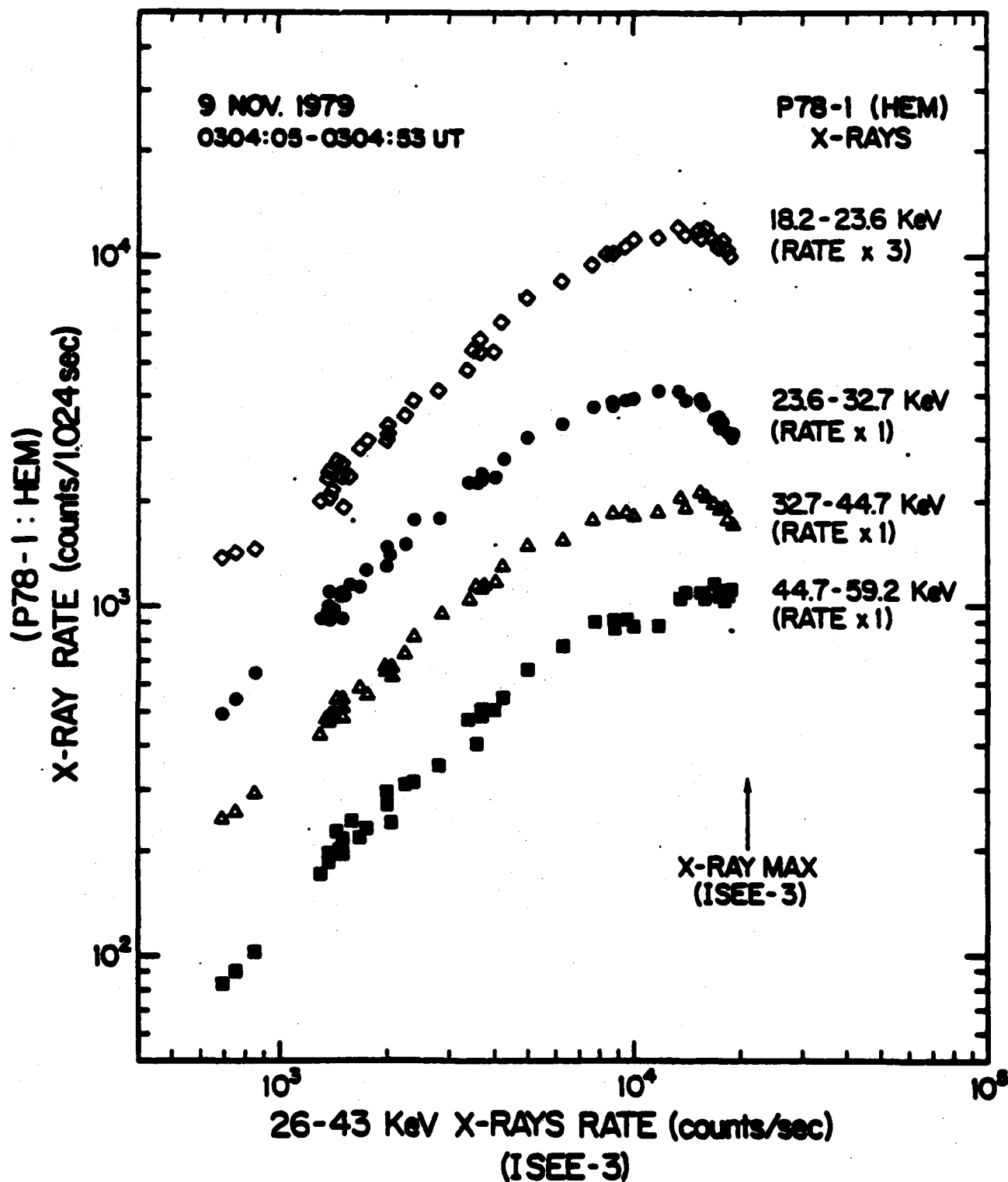
Figure 17: The HEM counting rates plotted against the ISEE-3 detector counting rate during a major solar flare. The HEM counting rates are saturated when the energy-integrated rate exceeds 10^4 s^{-1}.

and even undergoes a decrease. Since the HEM counting electronics has been designed to handle even higher counting rates, the saturation effect is probably caused by a decrease in the HEM detector gain. This is a well known effect of space charge build-up which is especially bad for a proportional counter containing a heavy gas (Xe) at high pressure (3 atmospheres) (Culhane et al., 1967).

VI. LIMITATIONS OF THE PRESENT ANALYSIS

Before the performance of the HEM can be properly evaluated, it is important to point out the following limitations of the present analysis:

1. The "standard" detector used for the in-flight calibration is the NaI(Tl) scintillator on the ISEE-3 spacecraft. The scintillator has an effective area of ~ 24 cm^2, comparable to the HEM detector area, and a large dynamic range. However the spectral resolution of the ISEE-3 scintillator is lower than that of the HEM proportional counter by a factor of ~ 2. The X-ray spectrum deduced from the ISEE-3 measurements has therefore a much larger uncertainty than that deduced from proportional counter measurements over a comparable energy range.

2. The incident X-ray spectrum has been assumed to be a double power law. The true solar flare spectrum could have a different shape (e.g., multi-thermal or thermal plus power law). In that case the procedure used here for comparing the HEM and ISEE-3 instruments may not be completely valid.

3. Although the gain of the HEM detector seems to have decreased after launch, the spectral resolution of the detector has been assumed to have maintained its pre-launch value. A change in the spectral resolution could affect the deduced gain of the detector significantly. The resolution of the detector has an important impact on the geometry factor at high γ. The workability of the present analysis may argue for the accuracy of the assumptions regarding resolution.

The present analysis represents a reasonable effort to deduce the HEM detector gain on the basis of the pre-launch characteristics of the HEM and a simple comparison of the HEM and ISEE-3 observations of seven solar X-ray

bursts. A more sophisticated analysis could involve extensive computer simulation and analysis. In view of the uncertainties and limitations mentioned above, it appears doubtful that such an extensive analysis will necessarily yield a more accurate evaluation of the instrument performance.

VII. SUMMARY AND CONCLUSIONS

The principal results obtained from this study are summarized as follows:

1. The gain of the HEM detector decreased monotonically and substantially after the launch of the P78-1 satellite. About 5 weeks after the launch, the gain was ~ 72% of its pre-launch value. About 15 months after the launch the gain was ~ 56%.

2. The detector response seems to saturate at total counting rates > 10^4 counts/sec. This is probably caused by a decrease in the detector gain at high counting rates.

3. The instrument gain was observed to increase with increasing applied high voltage, as expected.

The variation of detector gain after the launch is not uncommon in space instrumentation, especially in proportional counters. The relatively small rate of the long-term variation of the detector gain indicates that there is no significant leakage of the fill gas, and is possibly caused by anode degradation. The instrument is found to respond well to the changes in the high voltage. The counting electronics are apparently functioning well. The saturation effect at large counting rates is also common to most proportional counters and is therefore expected to occur. To summarize, the HEM instrument survived the spacecraft launch very well. Except for the change in the detector gain, the performance of the instrument is found to be satisfactory and hence the HEM measurements are expected to be useful for the study of many small and medium intensity solar X-ray bursts.

REFERENCES

Culhane, J. L., Sanford, P. W., Willmore, A. P., Blades, J., and Nettleship, R., 1967, IEEE Trans. Nuc. Sci., NS-14, 38.

Frost, K. J., and Dennis, B. R., 1971, Ap. J., 165, 655.

Kane, S. R., and Anderson, K. A., 1970, Ap. J., 162, 1003.

Kane, S. R., Crannell, C. J., Datlowe, D., Feldman, U., Gabriel, A., Hudson, H. S., Kundu, M. R., Matzler, C., Neidig, D., Petrosian, V., and Sheeley, Jr., N. R., 1980, in Solar Flares, (ed.) P. A. Sturrock, Colorado Assoc. Univ. Press, p. 187.

Kane, S. R., Fenimore, E. E., Klebesadel, R. W., and Laros, J. G., 1982, Ap. J. Letters (in press).

Landecker, P. B., Chater, W. T., Howey, C. K., McKenzie, D. L., Rugge, H. R., Williams, R. L., and Young, R. M., 1979, Aerospace Report SAMSO-TR-79-76, chapter 6.

Landecker, P. B., and McKenzie, D. L., 1981, Proc. Crimean Solar Max. Year Workshop, Simferopol, USSR, Vol. 1, p. 77.

Landecker, P. B., McKenzie, D. L., and Rugge, H. R., 1979, Proc. SPIE, 184, 285.

LABORATORY OPERATIONS

The Laboratory Operations of The Aerospace Corporation is conducting experimental and theoretical investigations necessary for the evaluation and application of scientific advances to new military space systems. Versatility and flexibility have been developed to a high degree by the laboratory personnel in dealing with the many problems encountered in the nation's rapidly developing space systems. Expertise in the latest scientific developments is vital to the accomplishment of tasks related to these problems. The laboratories that contribute to this research are:

Aerophysics Laboratory: Launch vehicle and reentry aerodynamics and heat transfer, propulsion chemistry and fluid mechanics, structural mechanics, flight dynamics; high-temperature thermomechanics, gas kinetics and radiation; research in environmental chemistry and contamination; cw and pulsed chemical laser development including chemical kinetics, spectroscopy, optical resonators and beam pointing, atmospheric propagation, laser effects and countermeasures.

Chemistry and Physics Laboratory: Atmospheric chemical reactions, atmospheric optics, light scattering, state-specific chemical reactions and radiation transport in rocket plumes, applied laser spectroscopy, laser chemistry, battery electrochemistry, space vacuum and radiation effects on materials, lubrication and surface phenomena, thermionic emission, photosensitive materials and detectors, atomic frequency standards, and bioenvironmental research and monitoring.

Electronics Research Laboratory: Microelectronics, GaAs low-noise and power devices, semiconductor lasers, electromagnetic and optical propagation phenomena, quantum electronics, laser communications, lidar, and electro-optics; communication sciences, applied electronics, semiconductor crystal and device physics, radiometric imaging; millimeter-wave and microwave technology.

Information Sciences Research Office: Program verification, program translation, performance-sensitive system design, distributed architectures for spaceborne computers, fault-tolerant computer systems, artificial intelligence, and microelectronics applications.

Materials Sciences Laboratory: Development of new materials: metal matrix composites, polymers, and new forms of carbon; component failure analysis and reliability; fracture mechanics and stress corrosion; evaluation of materials in space environment; materials performance in space transportation systems; analysis of systems vulnerability and survivability in enemy-induced environments.

Space Sciences Laboratory: Atmospheric and ionospheric physics, radiation from the atmosphere, density and composition of the upper atmosphere, aurorae and airglow; magnetospheric physics, cosmic rays, generation and propagation of plasma waves in the magnetosphere; solar physics, infrared astronomy; the effects of nuclear explosions, magnetic storms, and solar activity on the earth's atmosphere, ionosphere, and magnetosphere; the effects of optical, electromagnetic, and particulate radiations in space on space systems.

· · ·